

Pliocene four-rayed discoasters from IODP Expedition 363 sites in the eastern Indian Ocean and western Pacific Ocean

Allan Gil S. Fernando

National Institute of Geological Sciences, University of the Philippines, Diliman, Quezon City, 1101 Philippines; asfernando@up.edu.ph

Tom Dunkley Jones

School of Geography, Earth and Environmental Sciences, University of Birmingham, Edgbaston, Birmingham B15 2TT, UK; t.dunkleyjones@bham.ac.uk

Luc Beaufort

Aix Marseille Université, CNRS, IRD, INRAE, College de France, CEREGE, Aix-en-Provence, 13090, France; beaufort@cerege.fr

Denise K. Kulhanek

International Ocean Discovery Program, Texas A&M University, 1000 Discovery Drive, College Station, TX 77845, USA; kulhanek@iodp.tamu.edu

Yvonne Ivy L. Doyongan, Ana Marie E. Binuya, Jaan Ruy Conrad P. Nogot, Mirko Alessandro C. Uy

National Institute of Geological Sciences, University of the Philippines, Diliman, Quezon City, 1101 Philippines

Manuscript received 30th March, 2019; revised manuscript accepted 7th July, 2020

Abstract The stratigraphic distribution, occurrence and possible biostratigraphic significance of several previously-undescribed and rarely-reported four-rayed discoasters are described. The discoasters were observed in Zones NN10 to NN18 (Upper Miocene to Lower Pleistocene) in cores recovered from International Ocean Discovery Program Expedition 363 sites in the eastern Indian Ocean (offshore NW Australia) and western Pacific Ocean. One of the discoasters is a bilaterally-symmetrical form with simple ray-tip morphology, which is herein described as the new species *Discoaster alyssae*. Three new varieties are also introduced—*Discoaster surculus* var. *pullumpedes*, *D. variabilis* var. *pacificus* and *D. exilis* var. *resolutioniae*.

Keywords IODP Expedition 363, calcareous nannofossils, *Discoaster*, Late Miocene, Pliocene, Pleistocene

1. Introduction

Discoasters have been common components of calcareous nannofossil assemblages in marine sediments since their first known occurrence ~60 Ma (Late Paleocene; Bukry, 1971) until their extinction 1.93 Ma, during the Early Pleistocene (Gelasian; Raffi et al., 2006; Backman et al., 2012). Although Palaeogene discoasters usually have more than eight rays, Neogene discoasters typically only have five or six. Three- and four-rayed forms have also been reported, but the latter have been considered to represent inter- and intra-specific morphologic variability (Curry et al., 1995a) and/or ‘aberrant’ forms of known five- and six-rayed species (Curry et al., 1995b). Regardless of their origin, the three- and four-rayed forms can be relatively common constituents of nannofossil assemblages.

Based on data compiled in the online Nannotax3 database (<http://ina.tmsoc.org/Nannotax3>), four-rayed discoasters have been recorded from the Middle Miocene (Zone NN5 of Martini, 1971) to the Early Pleistocene

(NN18). Although some of the four-rayed discoasters are considered to be variants of previously-described taxa (e.g. *Discoaster surculus*, *D. exilis* and *D. petaliformis*), the majority of them are thought to be distinct species, identified on the basis of ray-tip morphology and central boss/structures, including *D. tamalis*, *D. blackstockiae*, *D. quadramus*, *D. styzenii*, *D. bolivariae*, *D. tetracladus* and *D. quadribollii*. With the exception of *D. tamalis*, most of these four-rayed species have not been used for biostratigraphic purposes. The four-rayed discoasters are usually bilaterally symmetrical, although interray angles of >90° have also been observed in some species/variants, resulting in asymmetrical forms (e.g. asymmetric *D. tamalis*, *D. styzenii* and *D. bolivariae*).

The shipboard calcareous nannofossil biostratigraphic investigation of sediments from International Ocean Discovery Program (IODP) Expedition 363 (Rosenthal et al., 2018a) sites in the eastern Indian Ocean (offshore NW Australia; Holes U1482A, U1482B, U1483A, U1483C)

and western Pacific Ocean (Holes U1486B, U1488A, U1489C, U1490A; Figure 1, Table 1) revealed the presence of several four-rayed discoasters, including one new species (*D. alyssae*). In this study, we described and documented the stratigraphic distribution and occurrence of *D. alyssae* and three new varieties—*D. surculus* var. *pullumpedes*, *D. variabilis* var. *pacificus* and *D. exilis* var. *resolutioniae*.

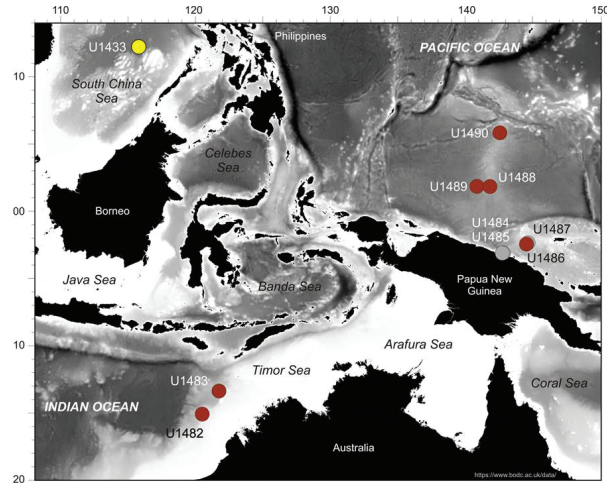


Figure 1: Bathymetric map, showing the location of the areas cored during IODP Expedition 363 (Western Pacific Warm Pool)—northwest Australian shelf (Sites U1482–U1483), Papua New Guinea/Manus Basin (Sites U1484–U1487) and the Eauripik Rise (Sites U1488–U1490). Red circles indicate sites where four-rayed, symmetrical discoasters were observed. Site U1433 in the South China Sea, cored during IODP Expedition 349 (South China Sea Tectonics), is also shown

Expedition	Location	Site	Coordinates	Water Depth (m)
349	South China Sea	U1433B	12.92N, 115.05E	4379.3
363	Indian Ocean (off NW Australia)	U1482A	15.06S, 120.44E	1467.7
		U1482B	15.06S, 120.43E	1464.5
		U1483A	13.09S, 121.80E	1732.9
		U1483C	13.09S, 121.80E	1731.2
	Pacific Ocean (Manus Basin)	U1486B	02.37S, 144.60E	1333.8
	Pacific Ocean (Eauripik Rise)	U1488A	02.04N, 141.75E	2603.4
		U1489C	02.12N, 141.03E	3423.7
		U1490A	05.82N, 142.65E	2341.0

Table 1: List of IODP sites, with locations where four-rayed discoasters were observed (Li et al., 2015; Rosenthal et al., 2018a)

2. Material and methods

The slides analysed during IODP Expedition 363 were prepared using the simple smear-slide method outlined in Bown & Young (1998). Onboard the research vessel *JOIDES Resolution*, the slides were examined using a Zeiss Axioscope light-microscope at 1000x magnification. Photomicrographs were taken using a SpotFlex camera, and IODP image-capture software. At the National Institute

of Geological Sciences, University of the Philippines (UP NIGS), the slides were observed using an Olympus BX51 polarising light-microscope at 1000x magnification. Photomicrographs were taken using Image-Pro Plus software installed on a computer attached to the microscope. The scanning electron microscope (SEM) images were taken using a Hitachi S3400-N SEM at UP NIGS.

The cores collected during IODP Expedition 363 are stored at the Gulf Coast Repository, College Station, Texas (USA). The smear-slides are stored at the UP, University of Birmingham and Aix-Marseille Université. The original digital images are archived in the laboratory information management system database of the IODP. Additional images are stored at the Nannoworks Laboratory, UP. The calcareous nannofossil range-charts of all the sites are included in Supplementary Table 1.

3. Results and discussion

Although *D. alyssae* was generally rare in our samples (one specimen per 11–100 fields of view), it was consistently recorded in NN15 to NN18 (upper Lower Pliocene to Lower Pleistocene) in the Indian Ocean and NN10 to NN18 (Upper Miocene to Lower Pleistocene) in the western Pacific Ocean (Figure 2, Table 2). In the South China Sea Site U1433B, *D. alyssae* was observed between NN16 and NN18 (Upper Pliocene to Lower Pleistocene).

Based on the available data, the base *D. alyssae* is coincident with the base paratype of *Reticulofenestra pseudoumbilicus* (8.79 Ma; Hilgen et al., 2012) and its top is coincident with the top *D. brouweri* (1.93 Ma; Hilgen et al., 2012). Although its top is the same at all sites, it is interesting to note its apparent earlier appearance in the western Pacific compared to the Indian Ocean and the South China Sea. The same ‘airplane’- or ‘chicken-foot’-like morphology was observed in other Pliocene species of *Discoaster* at IODP Expedition 363 sites, which are here described as new varieties of *D. exilis*, *D. variabilis* and *D. surculus* (Table 3). In the Gulf of Mexico, specimens of *D. pentaradiatus* and *D. bellus* with a similar irregular morphology have also been observed (David Bord, pers. comm., 2018). Whether these varieties represent specimens responding to changes in palaeoceanographic conditions (as in the case of *D. salisburgensis* during the Paleocene–Eocene Thermal Maximum; Bralower & Self-Trail, 2016) is outside of the scope of the present paper and will be explored in future studies.

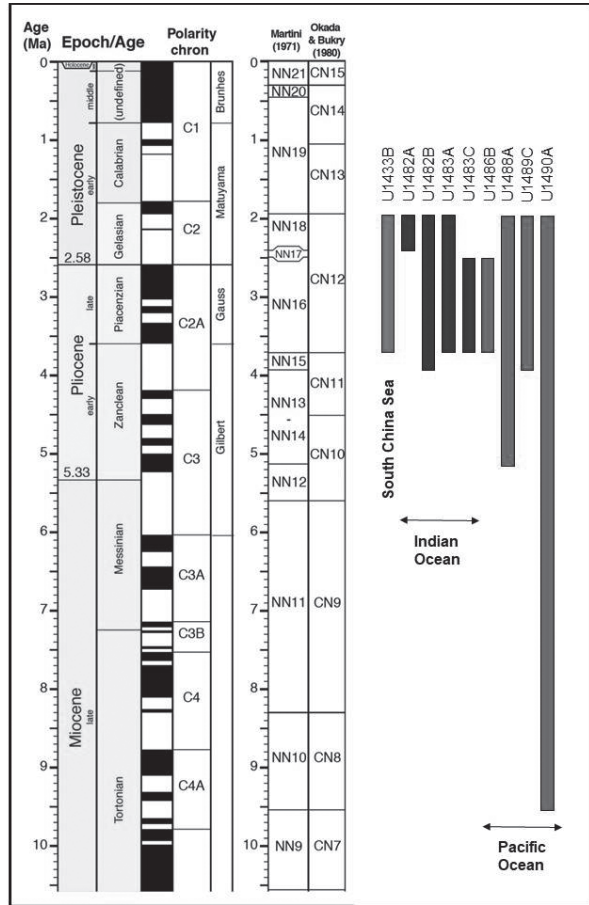


Figure 2: Stratigraphic distribution of *D. alyssae* sp. nov. in the Indian and Pacific Oceans and South China Sea. The bars represent the interval over which this species was observed at each site (see Table 2)

Site	Location	Occurrence		Nannofossil Zone (Age)
		Uppermost	Lowermost	
U1433B	South China Sea	12R-CC (286.14–286.24 m)	17R-3-W, 20/21 (333.05–333.06 m)	NN16–NN18 (Late Pliocene to Early Pleistocene)
U1482A	Indian Ocean (off NW Australia)	12H-2-W, 75/75 (100.16 m)	12H-CC (107.79–107.84 m)	NN18 (Early Pleistocene)
U1482B		13H-2-W, 51/51 (107.57 m)	18H-4-W, 51/51 (158.03 m)	NN15–NN18 (late Early Pliocene to Early Pleistocene)
U1483A		23H-CC (217.97–218.02 m)	31H-2-W, 50/50 (285.95 m)	NN16–NN18 (Late Pliocene to Early Pleistocene)
U1483C		24H-3-W, 117/117 (212.73 m)	—	NN16 (Late Pliocene)
U1486B	Pacific Ocean (Manus Basin)	22H-6-W, 81/81 (204.31 m)	—	NN16 (Late Pliocene)
U1488A	Pacific Ocean (Eauripik Rise)	6H-2-W, 60/60 (46.00 m)	14H-4-W, 60/60 (125.00 m)	NN13–NN15 (Early Pliocene to Early Pleistocene)
U1489C		5H-2-W, 60/60 (34.10 m)	9H-6-W, 60/60 (78.10 m)	NN15–NN18 (late Early Pliocene to Early Pleistocene)
U1490A		3H-6-W, 139/140 (22.29–22.30 m)	19H-5-W, 98/99 (172.45–172.46 m)	NN10–NN18 (Late Miocene to Early Pleistocene)

Table 2: Occurrence of *D. alyssae* sp. nov. in IODP Expedition 363 sites in the Indian and Pacific Oceans, and IODP Site U1433 in the South China Sea (IODP Expedition 349). The uppermost and lowermost occurrences, and the nannofossil zones and ages, are based on shipboard data combined with additional data generated by the authors

Compared to other four-rayed discoasters in the Miocene to Pliocene interval, *D. alyssae* has a longer geological range (Figure 3, and see references in Table 4). A similarity in ray-tip morphology suggests that *D. alyssae* could be a variety of *D. brouweri*. However, unlike the two four-rayed discoasters in the *D. brouweri* group (i.e. *D. tamalis* and *D. blackstockiae*), the fourth ray of *D. alyssae* is not in the same plane as the other three rays. The lack of recognition of *D. alyssae* in earlier studies may be due to its similarity to poorly-preserved/fragmented six-rayed discoasters that commonly exhibit detached or broken rays.

4. Systematic taxonomy

Family DISCOASTERACEAE Tan Sin Hok, 1927

Genus *Discoaster* Tan Sin Hok, 1927

Type-species *Discoaster pentaradiatus* Tan Sin Hok, 1927 (designated by Loeblich & Tappan, 1963, p. 192)

Discoaster alyssae sp. nov.

Pl. 1, figs 1–11, 16–19

Derivation of name: After Dr. Alyssa M. Peleo-Alampay (NIGS, UP), Filipino micropalaeontologist. **Diagnosis:** A species of *Discoaster* with four rays and simple, non-bifurcating, free ray-tips. **Description:** The angle between the three rays located on the same plane is ~120°, whereas the fourth ray is at an angle of usually <45° to the horizontal plane. This can create the appearance of the fourth ray being in the same plane as the other three rays. As a result, the discoaster appears to be bilaterally symmetrical. Morphologically, this species can be described as having an ‘airplane’ or ‘chicken-foot’ appearance. **Remarks:** *Discoaster alyssae* differs from the two other four-rayed discoasters in the *D. brouweri* group (*D. tamalis*, *D. blackstockiae*) in that the fourth ray is not in the same plane as the other three rays (Plate 1, figs 1–11). **Dimensions:** Length = 10–15.2 µm, width = 8.93–13.57 µm (based on 10 measured specimens). **Holotype:** Plate 1, figs 1, 2. **Paratypes:** Plate 1, figs 3, 4. **Type-locality:** IODP Hole U1489C, Eauripik Rise, western Pacific Ocean. **Type-level:** Upper Pliocene (NN16), Sample 363-U1489C-6H-CC (51.40–51.45 m). **Occurrence:** IODP Expedition 363 sites U1433, U1482A, U1482B, U1483A, U1483C, U1486B, U1488A, U1489C, U1490A; South China Sea (U1433B).

Site	Location	Discoaster variety	Occurrence		Nannofossil Zone (Age)
			Uppermost	Lowermost	
U1483A	Indian Ocean (off NW Australia)	<i>Discoaster exilis</i> var. <i>resolutioniae</i>	26H-6-W, 50/50 (243.99 m)	29H-CC (274.97-275.02 m)	NN16 (Late Pliocene)
U1488A	Pacific Ocean (Eauripik Rise)	<i>Discoaster exilis</i> var. <i>resolutioniae</i>	9H-2-W, 60/60 (74.50 m)	—	NN16 (Late Pliocene)
		<i>Discoaster surculus</i> var. <i>pullumpedes</i>	12H-2-W, 130/130 (103.70 m)	—	NN13-15 (Early Pliocene)
		<i>Discoaster variabilis</i> var. <i>pacificus</i>	12H-2-W, 130/130 (103.70 m)	—	NN13-15 (Early Pliocene)

Table 3: Occurrence of new varieties of *Discoaster* in IODP Expedition 363 sites in the Pacific and Indian Oceans. The uppermost and lowermost occurrences, as well as the nannofossil zones and ages, are based on a combination of shipboard data and additional data generated by the authors

currente: NN15 to NN18 (upper Lower Pliocene to Lower Pleistocene) in the Indian Ocean and NN10 to NN18 (Upper Miocene to Lower Pleistocene) in the western Pacific Ocean. In the South China Sea, in Hole U1433B, it was observed between NN16 and NN18 (Upper Pliocene to Lower Pleistocene).

Discoaster surculus var. *pullumpedes* var. nov.

Pl. 1, figs 12, 13

Derivation of name:

From the Latin ‘*pullum*’, meaning ‘chicken’, and ‘*pedes*’, meaning ‘foot’, referring to its ‘chicken-foot’-like morphology.

Diagnosis: A four-rayed variety of *D. surculus* that is bilaterally symmetrical, with interray angles of 120° and 60°. **Remarks:**

This new variety differs from the two other new varieties described in this paper in having trifurcate ray-tips (Plate 1, figs 12,

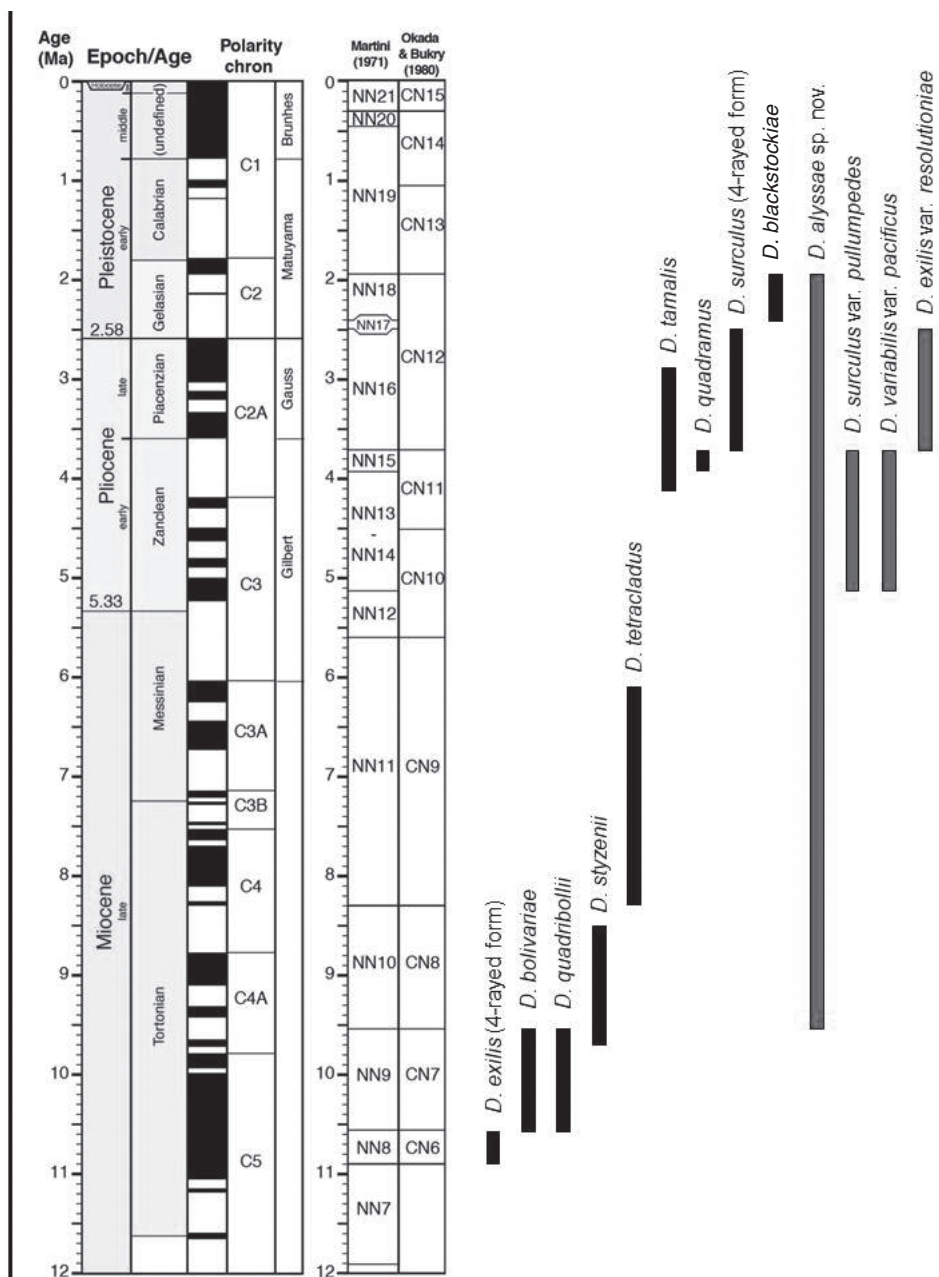


Figure 3: Stratigraphic range of Miocene to Pliocene four-rayed discoasters, *D. alyssae* sp. nov. and the three new discoaster varieties. Data from Nannotax (Young et al., 2019)

Species	Description	Stratigraphical Range	
<i>Discoaster blackstockiae</i> Bukry, 1973	Four-rayed variant of <i>D. brouweri</i> with inter-ray angles of 60° and 120°	Miocene to Pliocene (Bukry, 1973), NN18 (Browning et al., 2017)	Hole U1488A, Eauripik Rise, western Pacific Ocean. Type-level: Lower Pliocene (NN13–NN15), Sample 363-U1488A-12H-2-W, 130/130 (103.70 m). Occurrence: NN13–NN15 in the western Pacific Ocean.
<i>Discoaster bolivariae</i> Browning & Bergen in Browning et al., 2017	Four-rayed variant of <i>D. hamatus</i>	NN9, Late Miocene (Browning et al., 2017)	
<i>Discoaster exilis</i> Martini & Bramlette, 1963	Four-rayed variant	NN8, Late Miocene (Browning et al., 2017)	
<i>Discoaster petaliformis</i> Moshkovitz & Ehrlich, 1980	Four-rayed variant	NN5, Late Miocene (Theodoridis, 1984)	
<i>Discoaster quadramus</i> Bukry, 1973	Four-rayed variant of <i>D. pentaradiatus</i>	NN15, Pliocene (Young, 1998)	<i>Discoaster exilis</i> var. <i>resolutioniae</i> var. nov. Pl. 1, fig. 15
<i>Discoaster quadribollii</i> Browning & Bergen in Browning et al., 2017	Four-rayed variant of <i>D. bollii</i>	NN9, Late Miocene (Browning et al., 2017)	
<i>Discoaster styzenii</i> Wei, 2003	Four-rayed variant of <i>D. prepentaradiatus</i> (often asymmetrical)	NN9–NN10, Late Miocene (Browning et al., 2017)	
<i>Discoaster surculus</i> Martini & Bramlette, 1963	Four-rayed variant	NN16, Late Pliocene (Browning et al., 2017)	
<i>Discoaster tamalis</i> Kamptner, 1967	Symmetrical and asymmetrical four-rayed variety of <i>D. brouweri</i>	NN14–NN16, Pliocene (Young, 1998; Raffi et al., 2006)	
<i>Discoaster tetricladus</i> de Kaenel & Bergen in de Kaenel et al., 2017	Four-rayed variant of <i>D. quinqueramus</i>	NN11a, Late Miocene (Blair et al., 2017)	

Table 4: Description and stratigraphic range of four-rayed discoasters from the Miocene to Pliocene. Data compiled from Nannotax (Young et al., 2019)

13). It occurs within the geological range of *D. surculus* (NN11a–NN16; Young, 1998). **Dimensions:** Length = 12.5 µm, width = 10 µm (based on the holotype). **Holotype:** Plate 1, figs 12, 13. **Type-locality:** IODP Hole U1488A, Eauripik Rise, western Pacific Ocean. **Type-level:** Lower Pliocene (NN13–NN15), Sample 363-U1488A-12H-2-W, 130/130 (103.70 m). **Occurrence:** NN13–NN15 in the western Pacific Ocean.

Discoaster variabilis var. *pacificus* var. nov.

Pl. 1, fig. 14

Derivation of name: After the Pacific Ocean, where the variety was observed. **Diagnosis:** Four-rayed variety of *D. variabilis* that is bilaterally symmetrical, with interray angles of 120° and 60°. **Remarks:** This new variety differs from the two other varieties described in this paper in having rays with stronger and better-developed bifurcations (Plate 1, fig. 14). It occurs within the geological range of *D. variabilis* (NN10–NN16; Young, 1998). **Dimensions:** Length = 11.5 µm, width = 11 µm (based on the holotype). **Holotype:** Plate 1, fig. 14. **Type-locality:** IODP

it is bilaterally symmetrical, with interray angles of 120° and 60°. **Remarks:** This new variety differs from *D. variabilis* var. *pacificus* in having ray bifurcations that are acutely angled (Plate 1, fig. 15). This variety is younger than the known geological range of *D. exilis* (NN4–NN9; Young, 1998). **Dimensions:** Length = 13 µm, width = 11.5 µm (based on the holotype). **Holotype:** Plate 1, fig. 15. **Type-locality:** IODP Hole U1488A, Eauripik Rise, western Pacific Ocean. **Type-level:** Upper Pliocene (NN16), Sample 363-U1488A-9H-2-W, 60/60 (74.50 m). **Occurrence:** NN16 in the western Pacific and Indian Oceans.

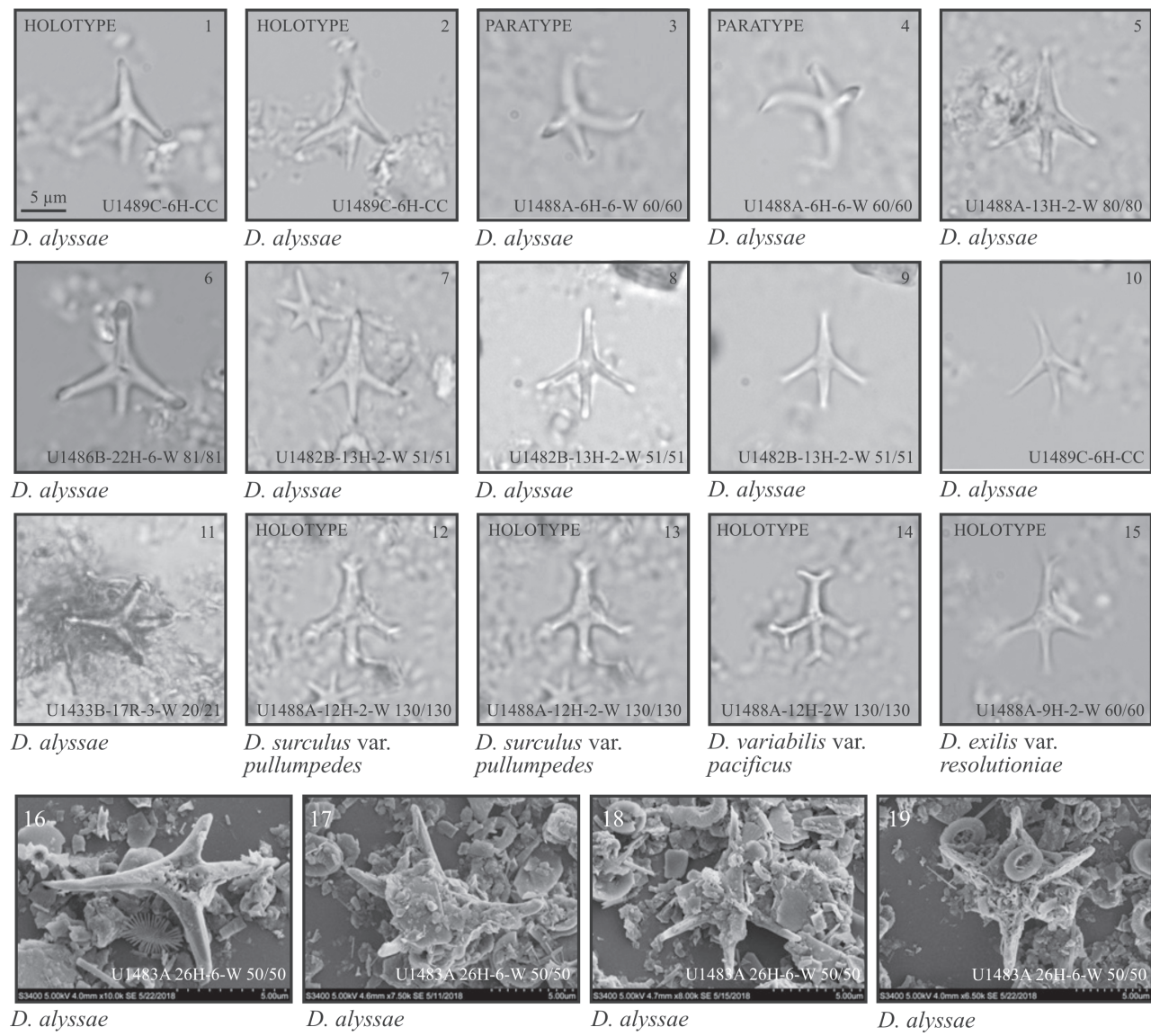
Acknowledgements

Samples for this study were provided by the IODP. The authors would like to thank the scientific party, staff and crew of IODP Expedition 363. The Nannoworks Laboratory of the NIGS, UP, is also acknowledged for use of their SEM. The comments of Jean Self-Traill and Laurel Bybell, which greatly improved the manuscript, are very much appreciated.

References

- Backman, J., Raffi, I., Rio, D., Fornaciari, E. & Pälike, H. 2012. Biozonation and biochronology of Miocene through Pleistocene calcareous nannofossils from low and middle latitudes. *Newsletters on Stratigraphy*, **45**(3): 221–244.
- Blair, S.A., Bergen, J.A., de Kaenel, E., Browning, E. & Boesiger, T.M. 2017. Upper Miocene–Lower Pliocene taxonomy and stratigraphy in the circum-North Atlantic Basin: Radiation and extinction of amauroliths, ceratoliths and the *D. quinqueramus* lineage. *Journal of Nannoplankton Research*, **37**(2–3): 113–144.
- Bown, P.R. & Young, J.R. 1998. Techniques. In: P.R. Bown (Ed.). *Calcareous Nannofossil Biostratigraphy*. British Micropalaeontological Society Publications Series, Chapman and Hall/Kluwer Academic Publishers, London: 16–28.
- Bralower, T.J. & Self-Trail, J.M. 2016. Nannoplankton malformation during the Paleocene–Eocene Thermal Maximum and its paleoecological and paleoceanographic significance. *Paleoceanography*, **31**: 1423–1439.
- Browning, E., Bergen, J.A., Blair, S.A., Boesiger, T.M. & de Kaenel, E. 2017. Late Miocene to Late Pliocene taxonomy and stratigraphy of the genus *Discoaster* in the circum-North Atlantic Basin: Gulf of Mexico and ODP Leg 154. *Journal of Nannoplankton Research*, **37**(2–3): 189–214.
- Bukry, D. 1971. *Discoaster* evolutionary trends. *Micropaleontology*, **17**(1): 43–52.
- Bukry, D. 1973. Phytoplankton stratigraphy, Deep Sea Drilling Project Leg 20, Western Pacific Ocean. *Initial Reports of the Deep Sea Drilling Project*, **20**: 307–317.
- Curry, W.B., Shackleton, N.J., Richter, C. et al. 1995a. Site 925. *Proceedings of the Ocean Drilling Program, Initial Reports*, **154**: 55–152.
- Curry, W.B., Shackleton, N.J., Richter, C. et al. 1995b. Site 926. *Proceedings of the Ocean Drilling Program, Initial Reports*, **154**: 153–232.
- de Kaenel, E., Bergen, J., Browning, E., Blair, S. & Boesiger, T. 2017. Uppermost Oligocene to Middle Miocene *Discoaster* and *Catinaster* taxonomy and biostratigraphy in the circum-North Atlantic Basin: Gulf of Mexico and ODP Leg 154. *Journal of Nannoplankton Research*, **37**(2–3): 215–244.
- Hilgen, F.J., Lourens, L.J. & van Dam, J.A. 2012. The Neogene period. In: F.M. Gradstein, J.G. Ogg, M.D. Schmitz & G. Ogg (Eds). *Geological Time Scale 2012*. Elsevier, BV 2: 923–978.
- Li, C.-F., Lin, J., Kulhanek, D.K. & the Expedition 349 Scientists. 2015. *Proceedings of the International Ocean Discovery Program*, **349**. *South China Sea Tectonics*, **349**.
- Loeblich, A.R. & Tappan, H. 1963. Type-fixation and validation of certain calcareous nannoplankton genera. *Proceedings of the Biological Society of Washington*, **76**: 191–196.
- Martini, E. 1971. Standard Tertiary and Quaternary calcareous nannoplankton zonation. In: A. Farinacci (Ed.). *Proceedings of the Second Planktonic Conference, Roma, 1970. Edizioni Tecnoscienza, Rome*, **2**: 739–785.
- Okada, H. & Bukry, D. 1980. Supplementary modification and introduction of code numbers to the low-latitude coccolith biostratigraphic zonation (Bukry, 1973; 1975). *Marine Micropaleontology*, **5**: 321–325.
- Raffi, I., Backman, J., Fornaciari, E., Palike, H., Rio, D., Lourens, L.J. & Hilgen, F.J. 2006. A review of calcareous nannofossil astrobiochronology encompassing the past 25 million years. *Quaternary Science Reviews*, **25**: 3113–3137.
- Rosenthal, Y., Holbourn, A.E., Kulhanek, D.K. & the Expedition 363 Scientists. 2018a. Western Pacific Warm Pool. *Proceedings of the International Ocean Discovery Program*, **363**. <https://doi.org/10.14379/iodp.proc.363.2018>
- Rosenthal, Y., Holbourn, A., Kulhanek, D. & the Expedition 363 Scientists. 2018b. Expedition 363 methods. *Proceedings of the International Ocean Discovery Program*, **363**. <https://doi.org/10.14379/iodp.proc.363.102.2018>
- Theodoridis, S. 1984. Calcareous nannofossil biostratigraphy of the Miocene and revision of the helicoliths and discoasters. *Utrecht Micropaleontological Bulletin*, **32**: 1–271.
- Young, J.R. 1998. Neogene. In: P.R. Bown (Ed.). *Calcareous Nannofossil Biostratigraphy*. Micropalaeontological Society Publication Series, Kluwer Academic Publishers, London: 225–265.
- Young, J.R., Bown P.R. & Lees J.A. 2019. Nannotax3 website. International Nannoplankton Association. Accessed 21 April, 2017. <http://www.mikrotax.org/Nannotax3>

Plate 1



The following tables were not included in the printed version of the paper but are given here in full. They are also available in Excel format (.xlsx) from the INA website

Supplementary Table 1: Calcareous nannofossil distribution, IODP 349, Hole U1433B (South China Sea)

Supplementary Table 2: Calcareous nannofossil distribution, IODP 363, Hole U1482A (Indian Ocean, off NW Australia)

Sample (Site U1482A)	Top Depth (m)	Bottom Depth (m)	Hannibalian Zone	Prevention	
				Abundance	Microbial activity
365.U1482A-110-11.0-W 55/50	2.00	2.00	NN21	G A	P R
365.U1482A-110-11.0-W 55/50	3.00	3.00		G D	R F
365.U1482A-120-2.5-W 55/50	4.00	4.00		G A	R F
365.U1482A-120-2.5-W 55/50	5.00	5.15		R F	F
365.U1482A-120-2.5-W 55/50	6.00	9.05		G A	R F
365.U1482A-120-2.5-W 55/50	10.00	12.75		R F	P
365.U1482A-120-2.5-W 55/50	14.00	14.65		G D	R F
365.U1482A-120-2.5-W 55/50	17.00	17.65		G D	R F
365.U1482A-120-2.5-W 55/50	20.00	20.65		G D	R F
365.U1482A-120-2.5-W 55/50	23.00	23.17		VG D	R F
365.U1482A-140-4.1-W 55/50	24.15	24.15	NN20	G D	R F
365.U1482A-140-4.1-W 55/50	27.15	27.15		G D	R F
365.U1482A-140-4.1-W 55/50	30.00	30.40		G A	R F
365.U1482A-140-4.1-W 55/50	30.64	30.69		G D	R F
365.U1482A-140-5.1-H 55/50	33.05	33.60		G D	A P
365.U1482A-140-5.1-H 55/50	35.00	35.20		G A	R F
365.U1482A-140-5.1-H 55/50	35.65	39.65		G D	R F
365.U1482A-140-5.1-H 55/50	40.97	41.02		G D	I P
365.U1482A-140-5.1-H 55/50	41.00	41.15		G D	R F
365.U1482A-140-5.1-H 55/50	44.15	46.15		G D	C P
365.U1482A-140-5.1-H 55/50	46.15	46.15	NN19	G D	C P
365.U1482A-140-5.1-H 55/50	49.15	49.15		G A	R F
365.U1482A-140-5.1-H 55/50	52.65	52.65		G A	C P
365.U1482A-140-5.1-H 55/50	53.65	53.65		G A	R F
365.U1482A-140-5.1-H 55/50	60.15	60.21		G D	R F
365.U1482A-140-5.1-H 55/50	62.15	62.15		G A	C P
365.U1482A-140-5.1-H 55/50	63.00	63.00		G D	R F
365.U1482A-140-5.1-H 55/50	68.17	68.17		G A	R F
365.U1482A-140-5.1-H 55/50	69.74	69.79		G D	I P
365.U1482A-140-5.1-H 55/50	70.00	70.00		G D	R F
365.U1482A-140-5.1-H 55/50	74.60	74.60	NN18	G D	R F
365.U1482A-140-5.1-H 55/50	77.69	77.69		G D	R F
365.U1482A-140-5.1-H 55/50	79.00	79.00		G D	R F
365.U1482A-140-5.1-H 55/50	81.15	81.15		G D	R F
365.U1482A-140-5.1-H 55/50	84.18	84.18		G D	R F
365.U1482A-140-5.1-H 55/50	85.20	86.20		G D	R F
365.U1482A-140-5.1-H 55/50	90.65	90.65		G D	R F
365.U1482A-140-5.1-H 55/50	93.85	93.95		M D	R F
365.U1482A-140-5.1-H 55/50	95.00	95.00		M D	R F
365.U1482A-140-5.1-H 55/50	98.07	98.12		M D	R F
365.U1482A-140-5.1-H 55/50	100.00	100.15	NN17	M D	I P
365.U1482A-140-5.1-H 55/50	101.00	101.00		M D	R F
365.U1482A-140-5.1-H 55/50	102.00	102.00		M D	R F
365.U1482A-140-5.1-H 55/50	105.15	106.19		M D	R F
365.U1482A-140-5.1-H 55/50	107.70	107.84		M D	R F
365.U1482A-140-5.1-H 55/50	109.00	109.00		M D	R F
365.U1482A-140-5.1-H 55/50	111.95	115.69		M D	R F
365.U1482A-140-5.1-H 55/50	115.95	115.95		M D	R F
365.U1482A-140-5.1-H 55/50	119.15	119.15		M D	R F
365.U1482A-140-5.1-H 55/50	122.15	122.17		M D	R F
365.U1482A-140-5.1-H 55/50	125.00	125.00	NN16	M D	R F
365.U1482A-140-5.1-H 55/50	128.82	128.87		M D	R F
365.U1482A-140-5.1-H 55/50	130.85	130.85		M D	R F
365.U1482A-140-5.1-H 55/50	133.00	133.00		M D	R F
365.U1482A-140-5.1-H 55/50	134.62	134.63		M D	R F
365.U1482A-140-5.1-H 55/50	138.20	138.25		M D	R F
365.U1482A-140-5.1-H 55/50	141.15	141.15		M D	R F
365.U1482A-140-5.1-H 55/50	144.15	144.18		G D	R F
365.U1482A-140-5.1-H 55/50	145.00	145.00		G D	R F
365.U1482A-140-5.1-H 55/50	147.60	147.65		G D	R F
365.U1482A-140-5.1-H 55/50	150.00	150.00	NN15	G D	R F
365.U1482A-140-5.1-H 55/50	153.00	153.00		M D	R F
365.U1482A-140-5.1-H 55/50	155.00	155.00		M D	R F
365.U1482A-140-5.1-H 55/50	157.00	157.00		M D	R F
365.U1482A-140-5.1-H 55/50	159.55	160.00		M D	R F
365.U1482A-140-5.1-H 55/50	162.00	162.00		M D	R F
365.U1482A-140-5.1-H 55/50	164.75	164.81		M D	R F
365.U1482A-140-5.1-H 55/50	174.22	174.34		M D	R F
365.U1482A-140-5.1-H 55/50	176.00	176.00		M D	R F
365.U1482A-140-5.1-H 55/50	178.55	180.05		M D	R F
365.U1482A-140-5.1-H 55/50	182.00	182.00	NN14	M D	R F
365.U1482A-140-5.1-H 55/50	202.31	202.56		M D	P
365.U1482A-140-5.1-H 55/50	207.60	207.65		M D	P
365.U1482A-140-5.1-H 55/50	210.67	210.67		M D	P
365.U1482A-140-5.1-H 55/50	213.87	221.21		M D	P
365.U1482A-140-5.1-H 55/50	231.48	231.53		M D	P
365.U1482A-140-5.1-H 55/50	235.40	239.45		M D	P
365.U1482A-140-5.1-H 55/50	259.53	259.53		M D	P
365.U1482A-140-5.1-H 55/50	262.75	262.75		VG D	P
365.U1482A-140-5.1-H 55/50	272.22	272.22		VG D	R
365.U1482A-140-5.1-H 55/50	278.65	278.65	NN13	VG D	R
365.U1482A-140-5.1-H 55/50	281.00	281.00		VG D	R
365.U1482A-140-5.1-H 55/50	297.72	297.77		VG D	R
365.U1482A-140-5.1-H 55/50	307.74	307.74		VG D	R
365.U1482A-140-5.1-H 55/50	329.78	329.83		VG D	R
365.U1482A-140-5.1-H 55/50	326.52	326.57		VG D	R
365.U1482A-140-5.1-H 55/50	329.02	329.07		VG D	R
365.U1482A-140-5.1-H 55/50	349.53	349.59		VG D	R
365.U1482A-140-5.1-H 55/50	354.62	354.68		VG D	R
365.U1482A-140-5.1-H 55/50	363.34	363.39		VG D	R
365.U1482A-140-5.1-H 55/50	368.75	368.80	NN12	VG D	R
365.U1482A-140-5.1-H 55/50	377.81	377.85		M D	R
365.U1482A-140-5.1-H 55/50	380.16	380.16		M D	R
365.U1482A-140-5.1-H 55/50	382.50	382.50		M D	R
365.U1482A-140-5.1-H 55/50	394.20	419.97		M D	R
365.U1482A-140-5.1-H 55/50	429.35	429.40		M D	R
365.U1482A-140-5.1-H 55/50	431.29	431.34		P D	R
365.U1482A-140-5.1-H 55/50	431.50	441.15		M D	R
365.U1482A-140-5.1-H 55/50	449.20	449.25		M D	R
365.U1482A-140-5.1-H 55/50	454.67	454.72		D A	R
365.U1482A-140-5.1-H 55/50	454.81	454.81	NN11	D A	R
365.U1482A-140-5.1-H 55/50	468.16	468.21		V G	R
365.U1482A-140-5.1-H 55/50	471.52	471.52		M D	R
365.U1482A-140-5.1-H 55/50	474.23	447.23		M D	R
365.U1482A-140-5.1-H 55/50	448.39	448.43		G D	R
365.U1482A-140-5.1-H 55/50	450.00	450.00		G D	R
365.U1482A-140-5.1-H 55/50	451.50	451.50		M D	R
365.U1482A-140-5.1-H 55/50	452.75	452.75		M D	R
365.U1482A-140-5.1-H 55/50	453.75	453.75		M D	R
365.U1482A-140-5.1-H 55/50	454.75	454.75		M D	R
365.U1482A-140-5.1-H 55/50	455.75	455.75	NN10	M D	R
365.U1482A-140-5.1-H 55/50	456.75	456.75		M D	R
365.U1482A-140-5.1-H 55/50	457.75	457.75		M D	R
365.U1482A-140-5.1-H 55/50	458.75	458.75		M D	R
365.U1482A-140-5.1-H 55/50	459.75	459.75		M D	R
365.U1482A-140-5.1-H 55/50	460.75	460.75		M D	R
365.U1482A-140-5.1-H 55/50	461.75	461.75		M D	R
365.U1482A-140-5.1-H 55/50	462.75	462.75		M D	R
365.U1482A-140-5.1-H 55/50	463.75	463.75		M D	R
365.U1482A-140-5.1-H 55/50	464.75	464.75		M D	R
365.U1482A-140-5.1-H 55/50	465.75	465.75	NN9	M D	R
365.U1482A-140-5.1-H 55/50	466.75	466.75		M D	R
365.U1482A-140-5.1-H 55/50	467.75	467.75		M D	R
365.U1482A-140-5.1-H 55/50	468.75	468.75		M D	R
365.U1482A-140-5.1-H 55/50	469.75	469.75		M D	R
365.U1482A-140-5.1-H 55/50	470.75	470.75		M D	R
365.U1482A-140-5.1-H 55/50	471.75	471.75		M D	R
365.U1482A-140-5.1-H 55/50	472.75	472.75		M D	R
365.U1482A-140-5.1-H 55/50	473.75	473.75		M D	R
365.U1482A-140-5.1-H 55/50	474.75	474.75		M D	R
365.U1482A-140-5.1-H 55/50	475.75	475.75	NN8	M D	R
365.U1482A-140-5.1-H 55/50	476.75	476.75		M D	R
365.U1482A-140-5.1-H 55/50	477.75	477.75		M D	R
365.U1482A-140-5.1-H 55/50	478.75	478.75		M D	R
365.U1482A-140-5.1-H 55/50	479.75	479.75		M D	R
365.U1482A-140-5.1-H 55/50	480.75	480.75		M D	R
365.U1482A-140-5.1-H 55/50	481.75	481.75		M D	R
365.U1482A-140-5.1-H 55/50	482.75	482.75		M D	R
365.U1482A-140-5.1-H 55/50	483.75	483.75		M D	R
365.U1482A-140-5.1-H 55/50	484.75	484.75		M D	R
365.U1482A-140-5.1-H 55/50	485.75	485.75	NN7	M D	R
365.U1482A-140-5.1-H 55/50	486.75	486.75		M D	R
365.U1482A-140-5.1-H 55/50	487.75	487.75		M D	R
365.U1482A-140-5.1-H 55/50	488.75	488.75		M D	R
365.U1482A-140-5.1-H 55/50	489.75	489.75		M D	R
365.U1482A-140-5.1-H 55/50	490.75	490.75		M D	R
365.U1482A-140-5.1-H 55/50	491.75	491.75		M D	R
365.U1482A-140-5.1-H 55/50	492.75	492.75		M D	R
365.U1482A-140-5.1-H 55/50	493.75	493.75		M D	R
365.U1482A-140-5.1-H 55/50	494.75	494.75		M D	R
365.U1482A-140-5.1-H 55/50	495.75	495.75	NN6	M D	R
365.U1482A-140-5.1-H 55/50	496.75	496.75		M D	R
365.U1482A-140-5.1-H 55/50	497.75	497.75		M D	R
365.U1482A-140-5.1-H 55/50	498.75	498.75		M D	R
365.U1482A-140-5.1-H 55/50	499.75	499.75		M D	R
365.U1482A-140-5.1-H 55/50	500.75	500.75		M D	R
365.U1482A-140-5.1-H 55/50	501.75	501.75			

Supplementary Table 3: Calcareous nannofossil distribution, IODP 363, Hole U1482B (Indian Ocean, off NW Australia)

Supplementary Table 4: Calcareous nannofossil distribution, IODP 363, Hole U1483A (Indian Ocean, off NW Australia)

Supplementary Table 5: Calcareous nannofossil distribution, IODP 363, Hole U1483C (Indian Ocean, off NW Australia)

Supplementary Table 6: Calcareous nannofossil distribution, IODP 363, Hole U1486B (Pacific Ocean, Manus Basin)

Sample Site (1486B)	Top Depth [m]	Bottom Depth [m]	Preservation	Abundance	Nanofossil Zone
363.U-1486B-24H-MLC	5.50	5.50			
363.U-1486B-24H-SW-5050	9.50	9.50			NN21
363.U-1486B-24H-SW-5050	12.50	12.50			NN20
363.U-1486B-24H-C	16.01	16.06			NN19
363.U-1486B-3H-3W-2050	18.65	18.65			NN18
363.U-1486B-3H-3W-2050	22.50	22.50			NN17
363.U-1486B-3H-FC-PM	25.32	25.42			NN16
363.U-1486B-4H-SW-5050	28.50	28.50			NN15
363.U-1486B-4H-SW-5050	31.50	31.50			NN14
363.U-1486B-4H-CC	35.05	35.10			NN13
363.U-1486B-4H-CC	39.75	39.75			NN12
363.U-1486B-5H-AW-7575	39.75	39.75			NN11
363.U-1486B-5H-AW-7575	42.75	42.75			NN10
363.U-1486B-5H-CC	44.40	44.45			NN09
363.U-1486B-5H-CC	53.88	53.93			NN08
363.U-1486B-5H-CC	55.20	55.20			NN07
363.U-1486B-7H-AW-120120	59.20	59.20			NN06
363.U-1486B-7H-AW-120120	62.81	62.88			NN05
363.U-1486B-8H-SW-130130	67.50	67.50			NN04
363.U-1486B-8H-SW-130130	70.30	70.30			NN03
363.U-1486B-8H-SW-130130	72.70	72.70			NN02
363.U-1486B-8H-SW-130130	74.46	74.46			NN01
363.U-1486B-9H-AW-9598	77.08	77.96			NN00
363.U-1486B-9H-AW-9598	80.96	80.96			RR09
363.U-1486B-9H-AW-9598	82.40	82.52			RR08
363.U-1486B-10H-W-120120	84.50	84.50			RR07
363.U-1486B-10H-W-120120	87.50	87.50			RR06
363.U-1486B-10H-W-120120	90.50	90.50			RR05
363.U-1486B-10H-W-120120	91.85	91.90			RR04
363.U-1486B-11H-2W-120120	94.20	94.20			RR03
363.U-1486B-11H-2W-120120	97.20	97.20			RR02
363.U-1486B-11H-AW-2020	100.20	100.20			RR01
363.U-1486B-11H-AW-2020	101.39	101.44			RP09
363.U-1486B-12H-1W-120120	103.50	103.50			RP08
363.U-1486B-12H-1W-120120	106.70	106.70			RP07
363.U-1486B-12H-1W-120120	109.20	109.20			RP06
363.U-1486B-12H-CZ	110.94	110.99			RP05
363.U-1486B-13H-2-W-110110	113.10	113.10			RP04
363.U-1486B-13H-2-W-110110	116.36	116.36			RP03
363.U-1486B-13H-2-W-110110	116.67	116.67			RP02
363.U-1486B-13H-2-W-110110	120.00	120.00			RP01
363.U-1486B-14H-2-SW-8383	122.33	122.33			RP00
363.U-1486B-14H-4-W-7272	125.22	125.22			RP09
363.U-1486B-14H-4-W-7272	128.45	128.45			RP08
363.U-1486B-14H-4-W-7272	129.50	129.50			RP07
363.U-1486B-14H-4-W-7272	130.20	130.20			RP06
363.U-1486B-14H-4-W-7272	133.02	133.02			RP05
363.U-1486B-15H-W-D4242	137.42	137.42			RP04
363.U-1486B-15H-W-D4242	140.50	140.50			RP03
363.U-1486B-14H-2-SW-8383	142.60	142.60			RP02
363.U-1486B-14H-2-SW-8383	142.90	142.90			RP01
363.U-1486B-14H-4-W-9595	144.80	144.94			RP09
363.U-1486B-14H-4-W-9595	146.80	146.84			RP08
363.U-1486B-14H-4-W-9595	149.80	149.84			RP07
363.U-1486B-14H-4-W-9595	152.80	152.84			RP06
363.U-1486B-14H-4-W-9595	155.80	155.84			RP05
363.U-1486B-14H-4-W-9595	158.80	158.84			RP04
363.U-1486B-14H-4-W-9595	161.80	161.84			RP03
363.U-1486B-14H-4-W-9595	164.80	164.84			RP02
363.U-1486B-14H-4-W-9595	167.80	167.84			RP01
363.U-1486B-15H-CC	169.71	169.71			RP09
363.U-1486B-15H-CC	170.71	170.71			RP08
363.U-1486B-15H-CC	171.71	171.71			RP07
363.U-1486B-15H-CC	175.71	175.71			RP06
363.U-1486B-15H-CC	176.71	176.71			RP05
363.U-1486B-15H-CC	177.50	177.50			RP04
363.U-1486B-15H-CC	178.50	178.50			RP03
363.U-1486B-15H-CC	179.50	179.50			RP02
363.U-1486B-15H-CC	180.50	180.50			RP01
363.U-1486B-16H-2-W-8585	185.35	185.35			RP09
363.U-1486B-16H-2-W-8585	186.95	187.00			RP08
363.U-1486B-16H-2-W-8585	194.45	194.45			RP07
363.U-1486B-16H-2-W-8585	196.02	196.02			RP06
363.U-1486B-16H-2-W-8585	198.59	198.59			RP05
363.U-1486B-16H-2-W-8585	204.31	204.31			RP04
363.U-1486B-22H-W-4040	205.74	205.79			RP03
363.U-1486B-22H-W-4040	205.90	205.90			RP02
363.U-1486B-22H-W-4040	M	F	R	R	RP01

Supplementary Table 7: Calcareous nannofossil distribution, IODP 383, Hole U1488A (Pacific Ocean, Eauripik Rise)

Supplementary Table 8. Calcareous nannofossil distribution, IODP 363, Hole U1489C (Pacific Ocean, Euxinik Rise)

Supplementary Table 9: Calcareous nannofossil distribution, IODP 363, Hole U1493A (Pacific Ocean, Easurpik Rise)